Local Physical Oceanographic Conditions During GasEx 2001

Gregory C. Johnson and Christopher L. Sabine
NOAA Pacific Marine Environmental Laboratory, Seattle, Washington

Draft manuscript for the *Journal of Geophysical Research*

Submitted version, 15 November 2002

Running Title:
JOHNSON ET AL.: GASEX 2001 LOCAL OCEAN CONDITIONS

Abstract. GasEx 2001 is a study of air-sea gas exchange in a region of CO_2 outgassing. The bulk of the experiment followed a drifting array of near-surface instruments. This array was deployed during the second half of February 2001 just south of the equator in the central Pacific ocean. Local physical oceanographic conditions during GasEx 2001 are analyzed using shipboard data and a simple one-dimensional mixed-layer model. A relatively warm, salty, oxygen-rich, nutrient-poor, and carbon-poor mixed layer is separated from the cold, fresh, oxygen-poor, nutrient rich, and carbon-rich equatorial thermostad by a strong and very salty thermocline centered near 70 m. The thermocline shoals about 13 m over the 15-day experiment, implying an upwelling rate of 1×10^{-5} m s^{-1}. Zonal velocity is surface-intensified and westward, with vertical shear mostly through the thermocline. Meridional velocity is also strongly sheared with a maximum equatorward flow in the thermocline that is nearly reversed by 17 m, suggesting the importance of Ekman dynamics. The mixed-layer model exhibits more near-surface warming over the course of the experiment than is observed. Prescribing upwelling in the model closes the heat budget within error estimates. Vertical shear of horizontal velocity within the mixed layer effects budgets by moving relatively warm, carbon-rich water northeastward at the mixed-layer base. Both entrainment and vertical shear of horizontal velocity within the mixed layer play a limited role in the mixed-layer carbon budget.

1. Introduction

GasEx2001 is a field experiment designed to study air-sea gas exchange in a region of net carbon outgassing. The bulk of the experiment involved measurements taken by and around a drifting array of near-surface instruments located in recently upwelled water in the central equatorial Pacific Ocean. This portion of the study started at 20:00 UTC February 13th 2001 (yearday 44.85) at 3.00^{o}S, 125.00^{o}W and continued for about 15.5 days until 08:00 UTC March 1st (yearday 60.32). By the end of the study the array had drifted to 2.30^{o}S, 131.54^{o}W, a distance of about 731 km (Figure 1). The NOAA Ship Ronald H. Brown was within a few km of the array throughout much of the experiment, continuously collecting shipboard Acoustic Doppler Current Profiler (ADCP) velocity data and shipboard meteorological data. The ship occasionally stopped to collect continuous profiles of temperature, salinity, and dissolved oxygen data as a function of pressure with a CTD/O_2 (Conductivity, Temperature, Depth, and Oxygen), as well as discrete water samples. From these water samples a variety of biogeochemically relevant water properties were measured. The ship also executed two regional butterfly surveys centered on the array near the start and the middle of the experiment. Each butterfly survey took slightly more than a day to complete. During these surveys the ship ranged as far as 80 km from the array. Large-scale oceanographic conditions surrounding this study are discussed elsewhere [*Johnson et al.*, 2002].

The budget of carbon in the mixed layer during the experiment is important for the study of air-sea flux measurements taken during the experiment. The mixed-layer carbon budget is of course sensitive to local physical oceanographic conditions including the evolution of the mixed layer. Here the CTD/O_2 and ADCP data are used to characterize local physical oceanographic conditions during the experiment. Water-mass property and velocity distributions, as well as their evolution, are described. Then CTD/O_2 profile data (together with Dissolved Inorganic Carbon, DIC, and nutrient data measured from water samples) are used to initialize a simple one-dimensional mixed-layer model [*Price et al.*, 1986; hereafter *PWP*] which is forced with shipboard meteorological measurements. The evolution of the model mixed layer is compared with observations. The model mixed layer warms slightly more than the observations indicate. Prescribing upwelling at the rate of thermocline shoaling in the model closes the mixed layer heat budget within air-sea flux estimate uncertainties. Entrainment of carbon-rich water from below into the mixed layer tends to increase DIC slightly within the mixed layer. The same process affects nutrient and oxygen budgets in the mixed layer. Differential horizontal advection within the mixed layer may also influence the mixed-layer carbon, nutrient, and oxygen budgets, and is discussed later.

2. Data

Forty-one CTD/O_2 casts were occupied as part of the main experiment (Figure 1). Data were taken from the surface to 500 dbar and processed to 1-dbar resolution. The CTD/O_2 data were calibrated using salinity and oxygen data analyzed from water samples collected with 23 bottles closed on each cast at about 17 nominal pressures, mostly located in the upper 100 dbar. Accuracy of the CTD/O_2 measurements is thought to be about 0.002^{o}C for temperature, 0.003 PSS-78 for salinity, better than 0.1% of full range, or 6 dbar, for pressure, and better than 1% of full range, or 2 μmol kg^{-1}, for oxygen. Casts were made near

the array at around 20:00 UTC, about local noon, (Figure 1) almost every day except during two regional butterfly surveys when 7 stations were occupied over about a day, many of these far from the array (Figure 1, ☆'s). During two different intensive sampling periods CTD/O_2 casts were taken every 3 hours in the vicinity of the array over a 24-hour period (Figure 1, x's). DIC measurements were made by coulometric titration from water samples, and are thought to be precise to about 2 μmol kg^{-1}. Nutrient measurements made by autoanalyzer from water samples are through precise to about 1% of full range , or 0.4 μmol kg^{-1} for nitrate (NO_3) and 0.03 μmol kg^{-1} for phosphate (PO_4).

ADCP velocity data were collected throughout the experiment, with one gap in the data lasting about 18 hours in the middle of the experiment. The data were processed in 5 minute by 8-m bins, with the first bin centered at 17 m and good data collected to nearly 450 m through much of the experiment. The data are thought to be accurate to at least 0.05 m s^{-1}. Variations in sound-speed, as determined by the calibrated CTD/O_2 data, were accounted for in the processing. Hourly averages of the data at the full 8-m vertical resolution are used here.

Meteorological data used here to force the one-dimensional mixed-layer model include the 10-m wind speed and direction, downwelling shortwave radiation, sea-surface albedo, downwelling longwave radiation, upwelling longwave radiation, bulk sensible heat flux, direct latent heat flux, and rain rate. These data are the best available estimates (as of May 1, 2002) of these quantities derived from measurements made with NOAA/ETL, WHOI, and resident instruments all mounted on the NOAA Ship Ronald H. Brown [*J. Edson and J. Hare,* personal communication 2002]. Net surface heat flux from such measurements are generally thought to be accurate to 10 W m^{-2}. The data are averaged in 30-minute bins.

3. Water mass and velocity structure

In this section the local temperature, salinity, and horizontal velocity fields are described. Large-scale observational and dynamical context for these fields is provided elsewhere [*Johnson et al.*, 2002]. The strong tropical thermocline shoals noticeably over the course of the experiment, suggesting upwelling. The salinity maximum within the thermocline is consonant with equatorward flow found there. The zonal flow, westward and surface intensified, shows the greatest increase within the thermocline, but continues to increase above it. This pattern contrasts with the meridional flow, which has the aforementioned equatorward maximum in the thermocline that is largely reversed at the shallowest measurement depth of 17 m. Thus, there is considerable vertical shear of horizontal velocity above the thermocline. Nonetheless, displacements estimated from the measured velocities are grossly consonant with drift path of the array.

The very strong tropical thermocline separates the warm near-surface layer (temperatures above 26°C) from the equatorial 13°C thermostad (Figure 2a). The thermocline is found between 60 m and 95 m at the start of the experiment. By the end of the experiment the thermocline is located between about 50 m and 85 m. The two intensive sampling periods near yeardays 47 and 57 reveal considerable short time-scale variability in thermocline depth, so the overall shoaling rate is estimated by a linear fit to depths of a set of potential isopycnals within the thermocline. These depths are found from the 29 CTD/O_2 casts occupied along the course of the array drift path (Figure 1, o's and x's), excluding casts taken far from the array during the regional butterfly surveys. This analysis suggests that the

thermocline shoals about 13 m over 15 days (1.0×10^{-5} m s^{-1}), following the mostly westward array drift of 715 km during that time. This upwelling rate is well within the range of short time scale variability in upwelling on the equator [*Weisberg and Qiao*, 2000], and the isotherm displacement is typical of the region.

The most pertinent feature in the salinity field (Figure 2b) is the salinity maximum embedded within the tropical thermocline. This maximum originates in the southern subtropics in a region of high evaporation and is advected equatorward within the South Equatorial Current [*Tsuchiya*, 1968]. This distinctive signature of mean equatorward flow within the thermocline contrasts with the fresher water above that is advected poleward in the mean by the near-surface flow [*Poulain*, 1993].

Zonal velocity during the experiment is surface intensified and westward (Figure 3a), as expected in the South Equatorial Current [*Wyrtki and Kilonsky*, 1984]. The zonal velocity at 25 m builds from near -0.2 m s^{-1} to -0.6 m s^{-1} during the course of the experiment. Mean westward flow during the experiment increases monotonically from 450 m to 17 m. The strongest vertical shear of zonal velocity is found in the thermocline, suggesting the likely importance of geostrophy. However, vertical shear associated with surface-intensification of westward velocity persists above the thermocline. Since easterly trades are predominant through the experiment, this near-surface vertical shear in zonal velocity is suggestive of the role of Ekman dynamics [*Price et al.*, 1987].

Like the zonal velocity, meridional velocity is weak below the thermocline, but it does not increase monotonically towards the surface (Figure 3b). Meridional velocity is increasingly northward up to the top of the thermocline, with strong vertical shear found within the thermocline. However, a reversal in the sign of this shear above the thermocline creates a clear maximum in northward flow that lies near the top of the thermocline. This maximum in northward flow is consonant with the salinity maximum found within the thermocline being advected northward from its southern subtropical source. By 17 m, the shallowest ADCP observation depth, the northward flow is much weaker in the mean, and occasionally reverses sign. Again, this tendency towards near-surface flow to the left (looking downwind of the easterly trades, and relative to the northward flow at the top of the thermocline) suggests the importance of Ekman dynamics.

Integration of the observed hourly averages of near-surface ADCP velocities over the course of the 15.5-day experiment to infer displacements at various depths during the experiment (Figure 4) quantifies the magnitude of the vertical shear of horizontal velocity. The large shear in the thermocline (between 105 m and 49 m) leads to increasing west-north-westward displacements with decreasing depth, and is likely largely geostrophic. However, above the thermocline (between 49 m and 17 m), the downwind (mostly westward) shear is reduced, and the displacements abruptly shift to the left of the (westward) wind stress (relative to the direction of presumably geostrophic flow within the thermocline) under the influence of Ekman dynamics. The vertical shear of horizontal velocity within the mixed layer would bring water at the mixed-layer base (say 33 m) northeastward by about 86 km relative to water nearer the surface (the shallowest observed values at 17 m). This significant upper-ocean vertical shear of horizontal velocity within the mixed layer may be important for mixed-layer budgets of heat and carbon, as discussed below.

The 17-m integrated displacement from the ADCP velocities falls about 127 km short of the mostly westward 731-km drift of the instrument array (Figure 4). Thus, the array is effectively drogued at some depth above 17 m. Linear extrapolation of observed shear

between the two shallowest ADCP measurement bins at 17 m and 25 m can be used to predict a displacement at 1-m depth (Figure 4) which is only about 60 km to the east of the final instrument array location. However, given the remaining shortfall, it is plausible that windage from the easterly trades on the array pushed it westward in relation to even the near-surface flow, so that the array was not truly Lagrangian at any depth. Given the uncertainty in extrapolating displacements from observed values to the surface, the array and the integrated near-surface flow measurements are in reasonable agreement. However, the discrepancy that remains could again be of importance for mixed-layer heat, carbon, nutrient, and oxygen budgets.

4. Mixed-layer model

To investigate the evolution of the mixed layer, a simple one-dimensional mixed-layer model [*PWP*] is run. The model is initialized with temperature and salinity profiles from the CTD/O_2 station occupied at the start of the experiment (Figure 1, eastmost o) and then forced for 15 days from the start of yearday 45 through the start of yearday 60 using heat, freshwater, and momentum fluxes estimated from shipboard meteorological measurements. Wind stresses are ramped up linearly from zero to observed values over the first three hours of the run to reduce initial transients. Water type Jerlov IB, with a shortwave attenuation depth of 17 m, is usually assumed to be typical of equatorial regions for the purposes of energy absorption [*Schudlich and Price*, 1992]. However, analysis of chlorophyll concentrations from the cruise following *Morel and Maritorena* [2001] results in a 25-m shortwave attenuation depth [*Strutton et al.*, 2002], so that value is used here. This substitution helps close the mixed-layer heat budget. The model domain extends from the surface to 500 m at 1-m intervals, and the model time step is set to 30 minutes, matching the averaging interval for the meteorological forcing.

Several modifications are made to the conventional *PWP* configuration. First, a weak background vertical diffusivity well below thermocline values [*Gregg*, 1998] is added, $k_z = 1 \times 10^{-6}$ m^2 s^{-1}. While this addition has little effect over the 15-day integration, it adds realism. Second, surface freshwater fluxes are applied and salinity is treated as an active variable. Third, passive tracers, including DIC, O_2, NO_3, and PO_4, are added and carried along in the model to investigate the role of entrainment in the mixed-layer budgets for carbon, oxygen, and nutrients in the absence of biological effects and air-sea gas exchange. Fourth, the full equation of state (EOS-80), rather than a linearized one more typical of *PWP* models, is used to calculate potential density and potential temperature, θ. Fifth, a maximum vertical velocity, $w = 1.0 \times 10^{-5}$ m s^{-1}, is prescribed in one of the two model integrations presented. This value is estimated from the thermocline shoaling of 13 m over 15.5 days as previously discussed. In the model w is assumed to increase linearly from zero at the surface to a maximum at the base of the mixed layer and then to decrease again to zero at the maximum model depth of 500 m. This simple upwelling pattern is expected from Ekman divergence in the mixed layer [*Schudlich and Price*, 1992].

To estimate an initial high vertical resolution DIC profile, a multiple linear regression of DIC is made to θ, salinity, apparent oxygen utilization, and unity [*Goyet and Davis*, 1997], using all the bottle data flagged as "good" from all the stations following the instrument array drift (Figure 1, o's and x's). The fit is done iteratively, discarding bottle data with residual magnitudes exceeding 2.8 times the residual standard deviation until no more data are

discarded. The iterations remove a few outlying values from the fit. Residuals of the 406 values which remain (95% of the initial 428) show only slight structure versus depth (Figure 5a). The final standard deviations of these residuals is only 3.1 μmol kg^{-1}, which is not much larger than the precision of the measurement. The resulting fit coefficients are applied to data from the initial 1-dbar vertical resolution CTD/O_2 profile to obtain a high-resolution DIC profile which agrees well with the DIC bottle data for that profile (Figure 5b). This high-resolution DIC profile is used to initialize the *PWP* model.

This same process is followed to obtain high-resolution NO_3 and PO_4 profiles. For the former, 355 out of the 381 bottles flagged good (91%) are retained in the final fit, which has a standard deviation of 0.5 μmol kg^{-1}. For the latter, 298 out of the 334 bottles flagged good (89%) are retained in the final fit, which has a standard deviation of 0.03 μmol kg^{-1}. These standard deviations correspond to the measurement precisions, suggesting good fits to the data. The high resolution O_2 profile is obtained directly from the CTD/O_2 data.

Of course the mixed-layer properties, especially temperature, exhibit significant diurnal variability owing to daily cycles in surface fluxes [*PWP*], and GasEx2001 is no exception. Thus the daily noon CTD/O_2 stations, and even the data from the two CTD/O_2 time-series, are not sufficient to evaluate the model performance for diurnal time-scales. Hence the more rapidly sampled shipboard sea-surface temperature (SST) is employed in this capacity. When the observed SST is compared with model results (Figure 6a), there is initial agreement as should be expected, but the model temperatures rise more quickly than the observed values. By yearday 59.65 the disagreement during the (night) time of coldest SST is around 0.1ºC for the model run without upwelling. (Using the Jerov IB 17-m shortwave attenuation depth instead of the 25-m value suggested by the chlorophyll data worsens agreement to 0.2ºC). For the model run with upwelling, the disagreement is reduced to about 0.04ºC. This remaining difference between modeled and observed SST could easily be accounted for by a surface heat flux bias well below the estimated accuracy of 10 W m^{-2}.

Every day the mixed-layer depth of the model with upwelling (Figure 6b) shoals to between 1 and 4 m (most frequently 3 m) in the late afternoon, because of the accumulated effects of near-surface daytime warming on the stratification. Every day the model mixed-layer depth is greatest, reaching between 8 m and 46 m on any given day, in the early morning, after night-time cooling and subsequent mixing. The most frequent maximum nocturnal mixed-layer depth is 32 m. Like the diurnal cycle in SST, this diurnal cycle in mixed-layer depth is typical [*PWP*]. The model without upwelling (not shown) exhibits very similar behavior in mixed-layer depth.

To qualitatively evaluate the overall evolution of the vertical structure of the model, temperature profiles are extracted from the model at the times near the start and end of the integration when CTD/O_2 stations were occupied. The initial profiles are in exact agreement (Figure 7) since the model is initialized using the CTD/O_2 profile. The observed profile occupied at yearday 58.89, close to the end the experiment and the integration, compares well with the corresponding model profile. Both reveal a thermocline that has shoaled about 13 m. In the model this shoaling is a direct result of the prescribed upwelling. Since the upwelling rate was estimated from the CTD/O_2 observations, the agreement is to be expected. Small vertical scale features visible in all the observed profiles and the initial model profile are not present in the later model profiles. These features have been smoothed out by the background vertical diffusion. Observed and modeled temperatures above the thermocline are also in fairly close agreement. While only just discernible given the large temperature scale in the

plot, temperature observations above the thermocline are cooler than the model by roughly 0.05ºC, with a local noon difference slightly larger than the early morning difference already discussed for the SST record. Thus, the gross modeled upper ocean structure agrees well with the observations over the course of the experiment. This agreement, as stated above, lies well within the likely uncertainty of measured surface heat fluxes.

Given the success in modeling the observed upper-ocean heat budget, we are emboldened to examine the effects of mixed-layer entrainment on the DIC budget through the temporal evolution of modeled DIC in the upper 30 m (Figure 8). This averaging depth is chosen as typical of the maximum nocturnal mixed-layer depth from examination of observed upper ocean profiles and the model results. For the model run without upwelling the mixed-layer DIC increases about 0.3 μmol kg^{-1} over the course of the experiment. For the run with upwelling, mixed-layer DIC increases about 0.4 μmol kg^{-1} over the course of the experiment. The inclusion of upwelling slightly enhances entrainment of deeper carbon-rich water into the mixed layer. The effects of entrainment over the first day of both model runs are larger than for the rest of the runs, likely because of spurious initial model transients. As a result, the model estimates of the effect of entrainment on the mixed-layer carbon budget might be biased high.

The corresponding calculations for O_2, NO_3, and PO_4, using output from the *PWP* model with prescribed upwelling, suggest mixed-layer enrichments of 0.3 μmol kg^{-1}, 0.04μmol kg^{-1}, and 0.005 μmol kg^{-1}, respectively for these quantities. The most unexpected of these results is for the oxygen, because the equatorial thermostad is oxygen-poor so one would anticipate that entrainment would decrease mixed-layer oxygen values. However, there is a slight increase of oxygen from the surface to a subsurface maximum near 50-60 m, and it is entrainment of water from these depths that results in a mixed-layer oxygen enrichment.

5. Discussion

A *PWP* mixed-layer model, initialized with CTD/O_2 and DIC observations, run with surface fluxes estimated from shipboard meteorological forcing, and using a shortwave attenuation depth derived from chlorophyll data, agrees fairly well with subsequent CTD/O_2 and SST observations, with the model trending slightly warmer than the observations over the course of the run. Agreement is improved to well within the uncertainties of the heat fluxes forcing the model by prescribing upwelling (estimated from observed thermocline shoaling) in the model. The upwelling obviously brings more cold water into the mixed layer, reducing model temperatures in the mixed layer. Since colder water is more carbon-rich, the upwelling also bring slightly more carbon (as well as nutrients and oxygen) into the mixed layer. The end result is a net increase in DIC of about 0.4 μmol kg^{-1} within the mixed layer over 15 days. However, other effects not accounted for in the one-dimensional model (aside from biology and gas exchange) might also be important in the mixed-layer property budgets.

One potential influence not included in the model is that of differential horizontal advection within the mixed layer (Figure 4). Two local butterfly surveys were completed around the floats as they drifted west, one immediately after the floats were deployed during yearday 45 and a second mid-way through the experiment during yearday 53 (Figure 1, ☆'s). The meridional and zonal gradients for those surveys are estimated from θ values at 30 dbar (a depth chosen to be within the mixed layer but below the effects of diurnal heating) and all DIC values above 32 dbar (Table 1). The gradients are estimated by fitting x-y planes to

these data. Errors are estimated from chi-squares calculated assuming 3 degrees of freedom (a 3 parameter fit applied to data from 7 distinct geographic locations) and the appropriate diagonal elements of the model covariance matrices. The errors on the fits are fairly large. All gradients but the meridional DIC values for the two surveys agree within their errors. Waters near the base of the mixed layer (33 m) move substantially east-northeast relative to the surface (1 m) water over the experiment duration. The differential meridional displacement of the observed displacement at 33 m is about 66 km northward over the course of the experiment relative to the extrapolated displacement at 1 m (Figure 1). The corresponding differential zonal displacement is about 138 km eastward over the 15.5 days.

Applying the mean of the gradients estimated from the two regional butterfly surveys to the lateral displacements estimated from the ADCP velocity data and dividing by two (to account for two end-member vertical mixing) allows estimates of the potential effects of differential lateral advection within the mixed layer owing to vertical shear of horizontal velocity. The values from the two surveys are averaged as differential advection persisted throughout the experiment. This calculation suggests that differential advection would tend to inject cool carbon-rich subsurface waters from the east-southeast under the surface waters. This injection would tend to destabilize the mixed layer and lead to a temperature change of +0.06 (±0.08) ºC over the course of the experiment. This change might tend to slightly increase the disagreement between observed and modeled SST, although the sign is uncertain given the error bars. For DIC the differential advective effects would result in a mixed-layer enrichment of about 1.3 (±1.7) µmol kg^{-1}. Both of these estimates are highly uncertain. First, the errors of lateral gradient estimates and the differences of those estimates between the two butterfly surveys are large. Second, the extrapolation of lateral displacements to the surface based on vertical shear of horizontal velocity observed between 17 m and 25 m is potentially fraught with error. This latter factor is not accounted for in the error estimate above.

This same calculation is applied to the O_2, NO_3, and PO_4 data. The end result for O_2 is a mixed-layer enrichment of 0.2 (±0.2) µmol kg^{-1}. That for NO_3 is the same. That for PO_4 is 0.003 (±0.006) µmol kg^{-1}. Again, these numbers are quite uncertain. However they do give some indication of the potential magntitude of the effect of differential horizonal advection within the mixed layer on mixed-layer property budgets.

Another potential effect on the mixed-layer properties observed by the drifting instrument array is the possibility that the array may not have exactly followed the surface waters, as discussed above. A comparison of the end point of the array and the displacement based on integration of ADCP velocities linearly extrapolated to 1-m depth (Figure 4) suggests that the array finished about 58 km west and 17 km north of the surface displacements. There is no regional survey at the conclusion of the experiment to asses the local gradients at that time and location. However, application of these distances to the surface gradients estimated from the second regional butterfly survey suggests that the instrument array mixed layer at the end of the experiment would not be significantly -0.00 (±0.08) ºC colder than it would be if the array were following the surface waters. In addition, the mixed layer sampled by the instrument array at the end of the experiment would be 1.1 (±1.4) µmol kg^{-1} poorer in DIC, -0 (±2) µmol kg^{-1} poorer in O_2, -0.2 (±0.1) µmol kg^{-1} poorer in NO_3, and -0.02 (±0.01) µmol kg^{-1} poorer in PO_4 had the array followed the drift of surface waters estimated from the ADCP data.

In summary, vertical entrainment at the base of the mixed layer likely slightly enriches the mixed layer with DIC (as well as nutrients and oxygen) over the course of GasEx2001.

Differential horizontal advection within the mixed layer likely has the same effect, although uncertainty is large. In addition, the slightly non-Lagrangain character of the drifting instrument array may mean that it finished in slightly DIC-richer (and nutrient-richer) water than it might have had it followed a surface water parcel. The sum of these three terms, however, is only 0.4 (±0.0)+ 1.3 (±1.7) -1.1 (±1.4) = 0.6 (±1.8) μmol kg^{-1} change in DIC. This net enrichment is a small value, with uncertainty the order of the precision of individual measurements. The reduction of mixed-layer DIC observed, on the order 6 μmol kg^{-1}, is significantly larger than (and of opposite sign to) changes due to the physical oceanographic processes considered here. Thus other effects (e.g. biology and gas exchange), appear to be dominant processes in the mixed-layer carbon budget during GasEx2001 [*Sabine et al.,* 2002].

Acknowledgements. This work was supported by the Global Carbon Program of the NOAA Office of Global Programs, the NOAA Office of Oceanic and Atmospheric Research, and the Joint Institute for the Study of the Atmosphere and Ocean (JISAO) under NOAA Cooperative Agreement No. NA17RJ11232,. The hard work of the ship's crew, and science party on the NOAA Ship Ronald H. Brown during GasEx2001 was essential. CTD/O_2 data were collected, calibrated and processed by Kristene McTaggart. Jules Hummon processed the ADCP data. Peter Strutton kindly shared his chlorophyll-based shortwave attenuation depth estimate. James Edson and Jeff Hare carefully worked up and generously shared the shipboard meteorological data. Marilyn Roberts analyzed the DIC data. Calvin Mordy and Charlie Fisher analyzed the nutrient and oxygen data. The mixed-layer model code was adapted from the notes for MIT/WHOI Joint Program course 12.747 [http://w3eos.whoi.edu/12.747/]. PMEL contribution 2528, JISAO Contribution 957.

References

Goyet, C. and D. Davis, Estimation of total CO_2 concentration throughout the water column, *Deep-Sea Research I, 44*, 859-877, 1997.

Gregg, M. C., Estimation and geography of diapycnal mixing in the stratified ocean, in *Physical Processes in Lakes and Oceans, Coastal and Estuarine Studies, Vol. 54*, edited by J. Imberger, pp. 305-338, 1998.

Johnson, G. C., K. E. McTaggart, and J. M. Hummon, Physical oceanographic conditions during GasEx2001: Large scale context, *J. Geophys. Res., submitted*, 2002.

Morel, A., and S. Maritorena, Bio-optical properties of oceanic waters: A reappraisal, *J. Geophys. Res., 106*, 7163-7180, 2001.

Poulain, P-M., Estimates of horizontal divergence and vertical velocity in the equatorial Pacific, *J. Phys. Oceanogr., 23*, 601-607, 1993.

Price, J. F., R. A. Weller, and R. Pinkel, Diurnal cycling: observations and models of the upper ocean response to diurnal heating, cooling, and wind mixing, *J. Geophys. Res., 91*, 8411-8427, 1986.

Price, J. F., R. A. Weller, and R. R. Schudlich, Wind-driven ocean currents and Ekman transport, *Science., 238*, 1534-1538, 1987.

Sabine, C. L., R. A. Feely, G. C. Johnson, P. G. Strutton, M. F. Lamb, K. E. McTaggart, and R. Wanninkhof, Carbon chemistry of the water column during GasEx-2001, *J. Geophys. Res., submitted*, 2002.

Schudlich, R. R., and J. F. Price, Diurnal cycles of current, temperature, and turbulent

dissipation in a model of the equatorial upper ocean, *J. Geophys. Res.*, *97*, 5409-5422, 1992.

Strutton, P. G., F. P. Chavez, R. C. Dugdale, and V. Hogue, Primary productivity and its impact on the carbon budget of the upper ocean during GasEx-2001, *J. Geophys. Res.*, *submitted*, 1992.

Tsuchiya, M., Upper waters of the intertropical Pacific Ocean, *Johns Hopkins Oceanogr. Stud.*, *4*, 50 pp., 1968.

Weisberg, R. H., and L. Qiao, Equatorial upwelling in the central Pacific estimated from moored velocity profilers, *J. Phys. Oceanogr.*, *30*, 105-124, 2000.

Wyrtki, K., and B. Kilonsky, Mean water and current structure during the Hawaii-to-Tahiti shuttle experiment, *J. Phys. Oceanogr.*, *14*, 242–254, 1984.

Table 1. Meridional and zonal gradients of potential temperature (θ) at 30 dbar and Dissolved Inorganic Carbon (DIC) above 32 dbar as estimated from the two regional butterfly surveys taken during days 45 and 53. Gradients are estimated by planar fits to the data from the two surveys and errors are derived from those fits assuming 3 degrees of freedom.

Survey	Θ gradient (10^{-3} ^{o}C km^{-1})		DIC gradient (μmol kg^{-1} km^{-1})	
	Zonal	Meridional	Zonal	Meridional
Butterfly 1	-0.3 (±1.9)	-2.6 (±1.9)	+0.03 (±0.04)	-0.11 (±0.03)
Butterfly 2	+0.3 (±1.0)	-1.1 (±1.0)	+0.01 (±0.02)	-0.04 (±0.02)

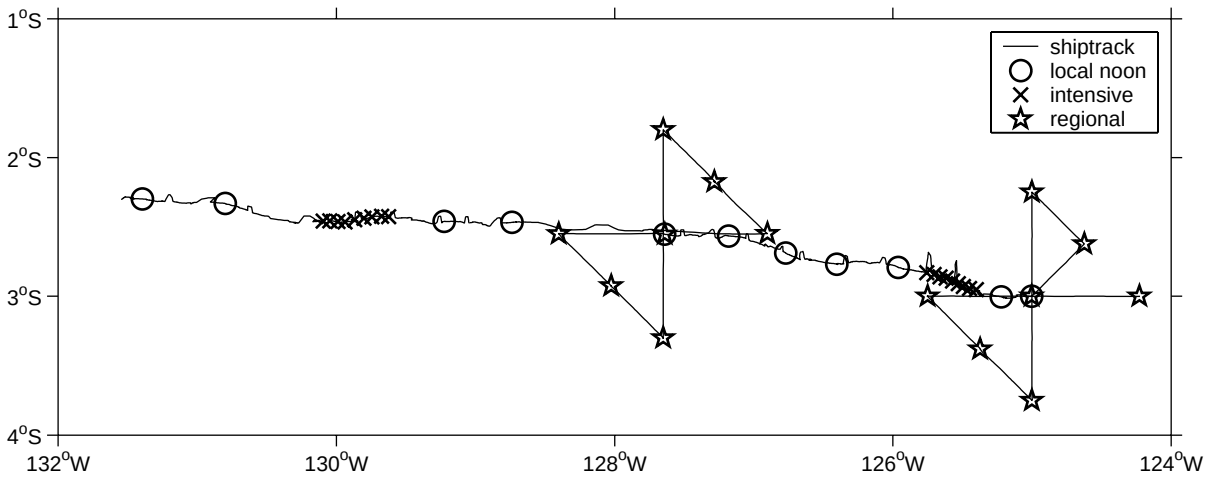

Figure 1. Ship track (solid line) and CTD/O_2 cast positions during GasEx2001 including noon casts following the instrument array drift (o's), casts taken following the array during the two intensive observation periods (x's), and casts taken mostly away from the array during the two regional butterfly surveys (☆'s).

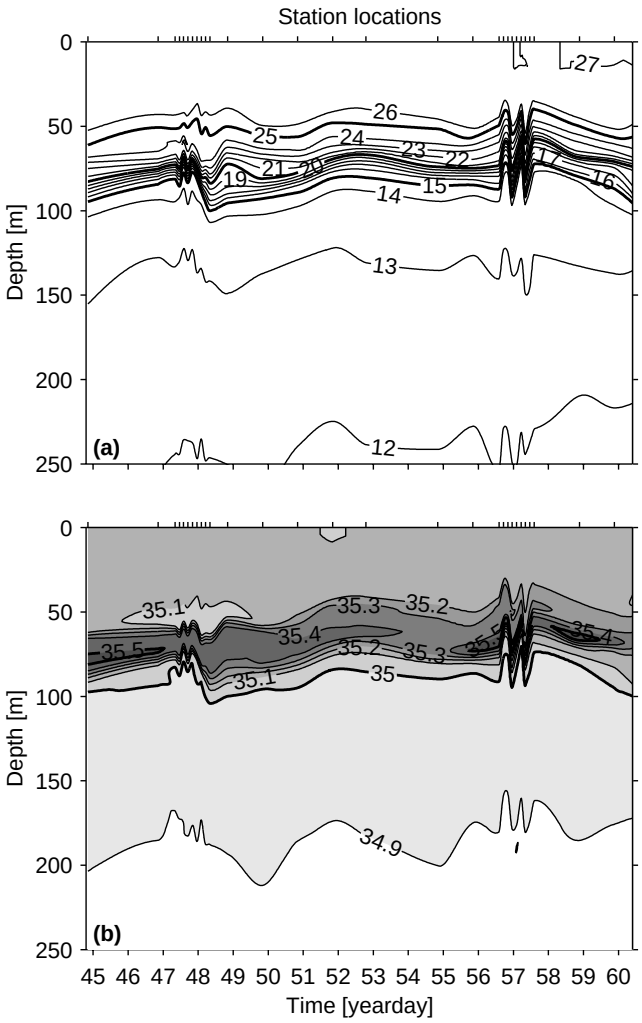

Figure 2. Vertical-temporal sections of data from CTD/O_2 casts occupied along the instrument array drift (Figure 1, o's and x's) contoured against time (yearday) and depth (m). (a) Potential temperature (θ) contoured at 1ºC intervals. (b) Salinity contoured at 0.1 (PSS-78) intervals with salty values increasingly shaded. Data have been vertically filtered with a 9-dbar Hanning filter for clarity of presentation. Ticks along the top axis show station times.

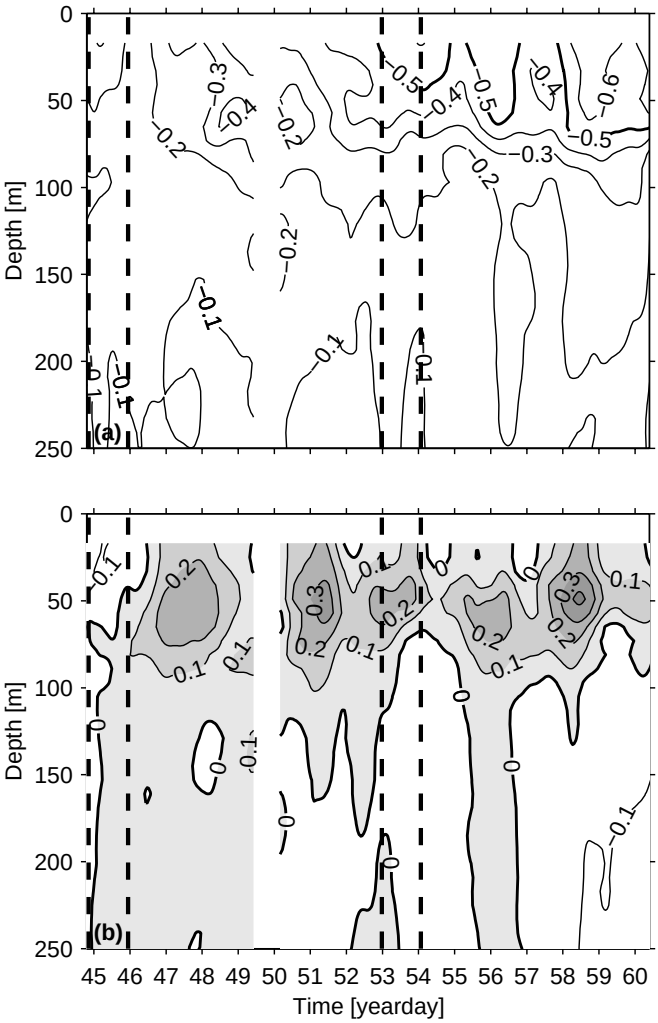

Figure 3. Vertical-temporal sections of (a) zonal velocity and (b) meridional velocity contoured at 0.1 m s^{-1} intervals against time (yearday) and depth (m) with positive values increasingly shaded. The data are smoothed temporally using a low-pass filter with a 24-hour half-power point for clarity of presentation. A data gap of 18 hours starting during yearday 49 is left uncontoured. Unlike Figure 2, data taken during the regional butterfly surveys are included. These surveys (delimited by thick dashed vertical lines around days 45 and 53) take about a day and range as far as 80 km from the drift of the instrument array.

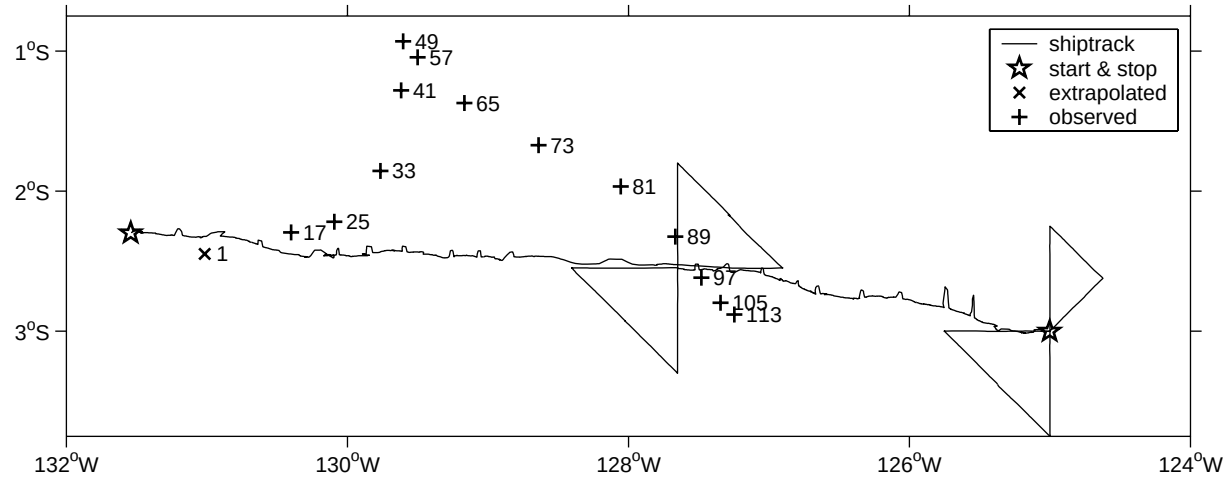

Figure 4. Displacement diagram made by integrating observed ADCP velocities at observed depths over the 15.5-day course of the experiment (+'s with depths labeled) with the ship-track over the course of the experiment (solid line) from initial deployment of the drifting instrument array to final recovery (☆'s) shown for reference. The 18-hour gap in ADCP velocities during yearday 49 (Figure 3) is filled by linearly interpolation. A surface displacement (x with depth labeled) is estimated by linearly extrapolating displacements between the two shallowest measured depths of 17 m and 25 m to 1-m depth.

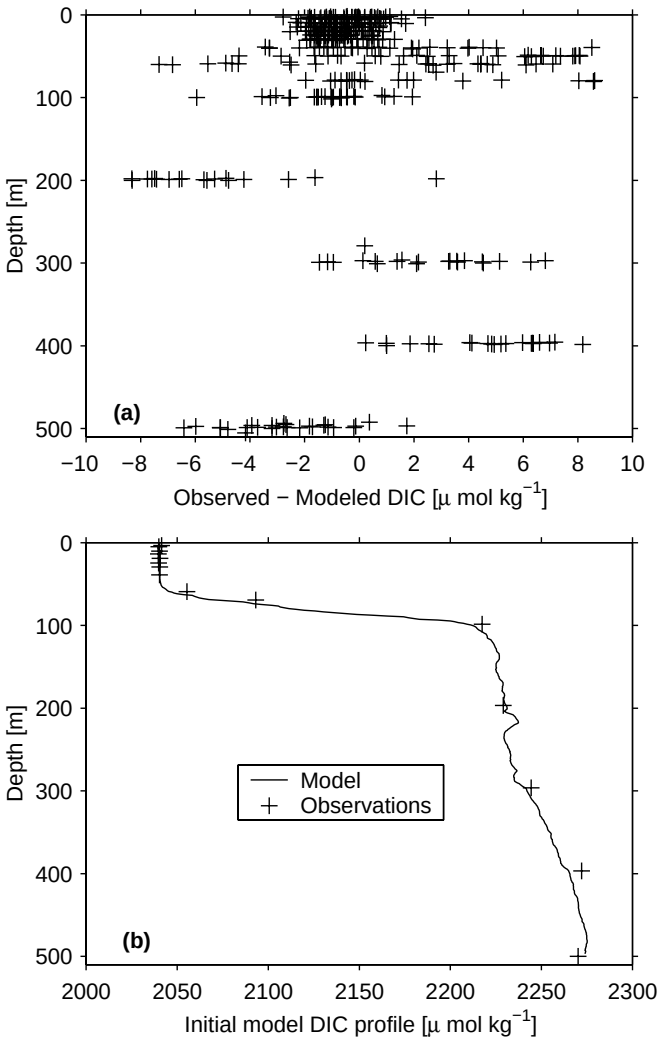

Figure 5. (a). Residuals (observations - model) of Dissolved Inorganic Carbon (DIC; μmol kg^{-1}) for a multiple linear regression against potential temperature, salinity, apparent oxygen utilization, and unity plotted against depth [m]. (b). Initial model high-resolution profile of DIC (solid line) plotted against depth constructed by applying the regression parameters to data from the first CTD/O2 station along the instrument drift track. DIC bottle data from that same station (+'s) are in good agreement with the initial model profile.

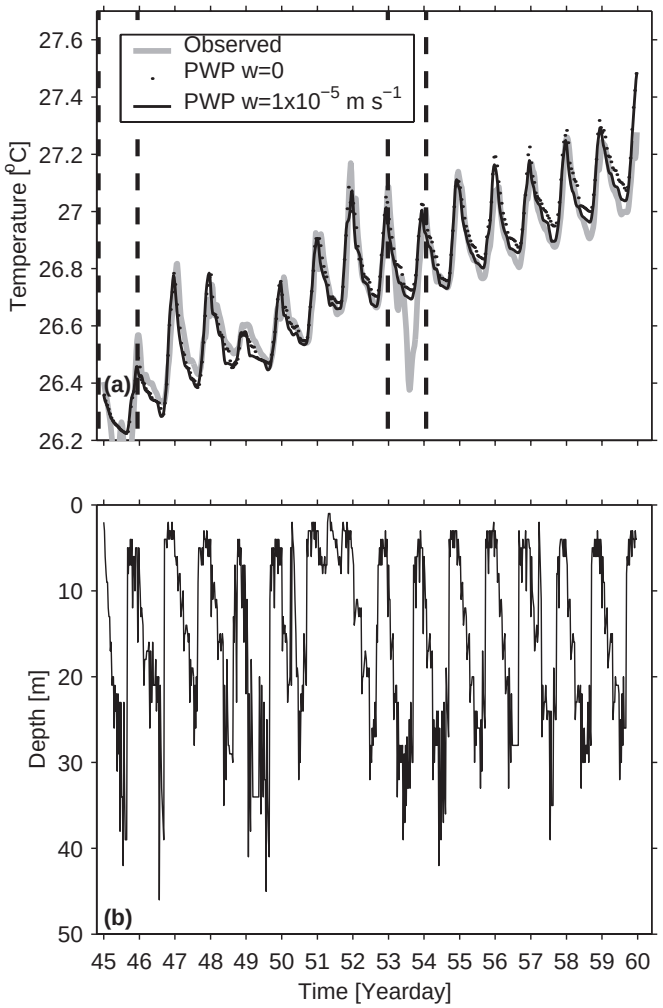

Figure 6. (a) Shipboard sea-surface temperature (SST; °C) plotted versus time (thick grey line). Data are smoothed using a low-pass filter with a 3-hour half-power point for clarity of presentation. Identically smoothed SSTs from *PWP* model integrations without (dotted line) and with (thin black line) prescribed upwelling are shown for comparison. Regional surveys when the ship departs from the drifting instrument array are delimited with thick dashed vertical lines around days 45 and 53. (b) Modeled mixed-layer depth from the integration with prescribed upwelling plotted versus time with no smoothing.

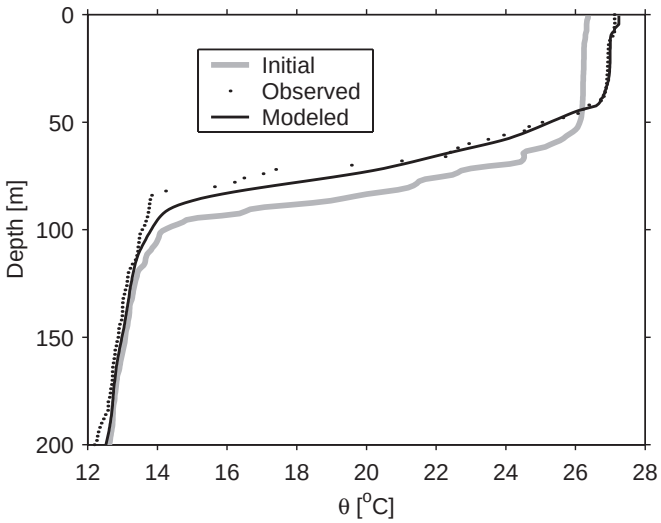

Figure 7. Initial observed and modeled potential temperature (θ; °C) profiles versus depth (m) exactly overlap since the model is initialized with observations (thick grey line). The observed θ profile taken at yearday 58.89 (dotted line) is also in good agreement with the corresponding model θ profile (thin black line).

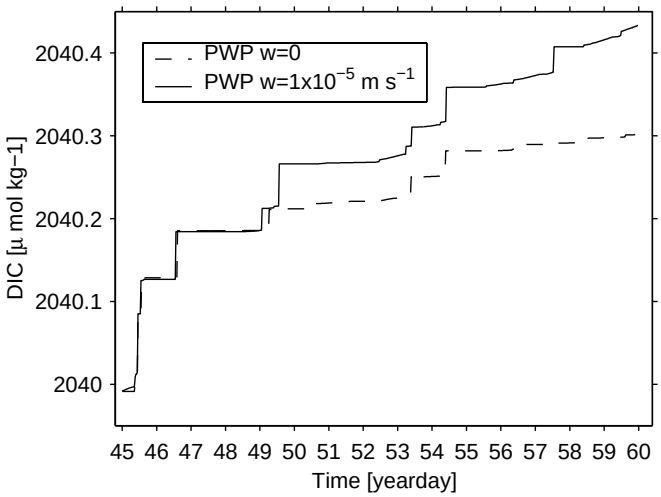

Figure 8. Modeled Dissolved Inorganic Carbon (DIC; µmol kg^{-1}) averaged over the top 30 m of the water column for the model runs without (dashed line) and with (solid line) upwelling plotted versus time.